DOI: 10.1021/ma901712s

Macromolecules
ARTICLE

Effect of Precursor Molar Mass on the ^{2}H NMR Line Shapes of End-Linked PDMS Elastomers

Geoffrey D. Genesky, T. M. Duncan, and Claude Cohen*

School of Chemical and Biomolecular Engineering, Olin Hall, Cornell University, Ithaca, New York 14850

Received July 31, 2009; Revised Manuscript Received October 2, 2009

ABSTRACT: A series of end-linked PDMS networks synthesized with different molar mass precursor chains is examined using ^{2}H NMR spectroscopy. The resulting line shapes for networks in the undeformed state show clear differences with precursor chain molar mass. Furthermore, samples uniaxially extended to high extension ratio show a clear shoulder in the line shape and two characteristic splittings (two doublets). Comparison with spectra for deuterated free chains dissolved in an unlabeled network confirms that the inner doublet results from excluded volume interactions between segments whereas the outer doublet is due to more highly aligned chain segments from chains with conformations trapped by the cross-linking reaction.

1. Introduction

To understand molecular-level structure in elastomers, it is important to directly probe the network properties at local scales. ^{2}H NMR has been utilized for this purpose because it allows for examination of chain segment orientation through the deuterium quadrupole interaction.[1−11] In polymers, deuterium nuclei are typically covalently bonded to carbon atoms. Each deuterium has a quadrupolar moment that interacts with the component of the electric field gradient directed along the C−^{2}H bond. The distribution of C−^{2}H orientations is controlled by the distribution of orientations of the polymer backbone. Therefore, since ^{2}H NMR measures the quadrupolar interaction at each C−^{2}H bond, it is a tool to directly examine the orientations of polymer chain segments.[12] When segments are randomly oriented and their motion is fixed on the time scale of the NMR experiment, a Pake pattern is observed.[13] This well-known line shape, which is found for rigid solids, has an overall line width on order 100 kHz. When segmental motion increases and the motion is isotropic, like in the case of low molar mass polymer melts, significant averaging of the quadrupolar interaction occurs, and the spectrum narrows into a sharp peak.

Elastic chains cross-linked into a network structure are an intermediate case between rigid solids and melts. While the motion of the segments is fast and the line width is orders of magnitude narrower than the Pake pattern, the spectra are still significantly broader than those of un-cross-linked melts. Past experiments[3,4] have demonstrated "wings" in the spectra which correspond to a super-Lorentzian line shape (Figure 1). Therefore, the constraints imposed by the cross-links cause non-isotropic motion corresponding to a residual quadrupolar frequency distribution when compared to the melt state. For any single, fixed orientation of a C−^{2}H bond, the resulting NMR spectrum is two lines spaced equally about zero frequency. The magnitude of this separation $\delta\nu_Q$ is given by[13]

$$\delta\nu_Q = 3/4\delta_Q(3\cos^2\theta - 1) \quad (1)$$

where δ_Q is the quadrupolar coupling constant and θ is the angle between the C−^{2}H bond and the magnetic field B_0. In a labeled elastic network, however, C−^{2}H bonds are oriented at all possible angles with the magnetic field, and these orientations are constantly fluctuating due to segmental motion. Therefore, the NMR spectrum of an undeformed elastomer is a time-averaged sum of the pair of lines corresponding to each C−^{2}H bond.

When a deuterium-labeled network is deformed uniaxially, more elastic chain segments are aligned with the strain axis. Therefore, the motional averaging of the quadrupolar interaction is no longer spatially isotropic, and the NMR spectrum broadens inhomogeneously. When the applied stress becomes high enough, the time-averaged sums of the pairs of lines described by eq 1 become disparate enough such that two peaks become visible. The distance between these two peaks is termed the splitting $\Delta\nu$ (Figure 1). As the spectrum broadens with increasing elongation ratio α, the distance between the peaks also increases.

The instantaneous contribution to the line shape for any given segment of an elastomer strained perpendicular to the external magnetic field is given by[6]

$$\delta\nu = 3/4\delta_Q P_2(\cos\phi)P_2(\cos\psi) \quad (2)$$

where $\delta\nu$ is the doublet separation, ϕ is the angle between the chain segment vector and the C−^{2}H bond, ψ is the angle between the segment vector and the applied strain, and $P_2(\cos x)$ is the second Legendre polynomial of $\cos x$.

The order parameter used to quantify segment anisotropy, S, is defined as

$$S = \langle P_2(\cos\psi)\rangle \quad (3)$$

where the brackets indicate an average over all chain segments. Comparison with eq 2 reveals that $\delta\nu$ is directly proportional to S. Classical elastic theories[14,15] predict a direct dependence of S on $\alpha^2 - 1/\alpha$, and thus the distance between the peaks $\Delta\nu$ is often correlated with this elongation ratio-dependent term. However, just as in the undeformed case, the total spectrum of a strained elastomer is the sum of the contributions from each labeled bond, averaged over time. Therefore, the locations of the peaks represent the most frequently accessed degree of segment orientation and not the average segment orientation ($\Delta\nu$ does not correspond to the average $\delta\nu$). To obtain the average segmental orientation,

*To whom correspondence should be addressed.

 Published on Web 10/09/2009

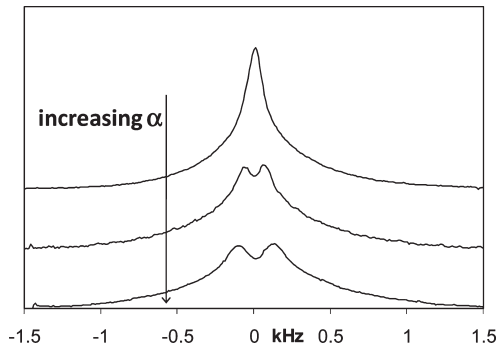

Figure 1. "Super-Lorentzian" line shape of our undeformed PDMS elastomer splits into two peaks equidistant from zero frequency with increasing elongation ratio α compared to unstretched state.

one needs to consider the entire line shape of the ^{2}H NMR spectrum, including the spectral wings.

Several mathematical models have been proposed to analyze the contributions to the ^{2}H NMR line shape. A uniaxial mean field model was used to replicate the orientational coupling between chain segments.[16] Results of this treatment indicate that the doublet disappears when the field is absent, and the network chains thus become noninteracting ("phantom" chains). Alternatively, the splitting has been reproduced by introducing a term that creates an anisotropic attractive potential upon strain to mimic the screening of excluded volume interactions between segments.[17,18] This theoretical model shows reasonable agreement with polybutadiene network line shapes at low strain.[19] Therefore, segment−segment interactions appear to have a considerable influence on the splitting $\Delta\nu$. These observations have been corroborated by Monte Carlo (MC) simulations of rubbery networks, where the mean field was introduced as an excluded volume effect between chain segments.[20,21] Further MC work demonstrated identical $\Delta\nu$ values upon stretching for both elastic chains and free chains dissolved in a network, but a higher average total order for the elastic chains.[22] These analyses and experimental results led to several models that attempted to describe the entire spectrum in terms of contributions from two different segment populations.[23−26] In their computer simulation study of NMR line shapes of perfect networks (no defects) under increasing strain, Yong and Higgs observed that the central split of the spectra correlates with chain interaction and packing whereas the outer wings result from highly extended chains with initially large end-to-end distances.[27] Networks of noninteracting ("phantom") chains exhibited only a widening of the spectral line under strain and no split. Additionally, the authors found that proximity to cross-link points had very little effect on the line shape contribution.

In this paper, we obtain and describe the evolution of the ^{2}H NMR spectra for elastic chains as a function of the precursor chain length (or cross-link density). Such a study of model end-linked unimodal networks with a systematic variation of the precursor chain molar mass has not been performed and reveals the role of the cross-link constraints on the NMR spectra. Line shape analysis of the end-linked PDMS networks allows us to probe the segment orientation of the elastic chains of different chain sizes in the undeformed state. We also examine stretched networks, where a shoulder appears in the spectra at high strain. This may indicate different populations of averaged segment orientations, which are empirically fit to two pairs of curves. We do not imply that there are two distinct types of chains, but rather that the segment orientation may be influenced primarily by either excluded volume interactions or by constraints imposed by the cross-links. To compare the spectra of elastic chains which are constrained on both ends to those of unconstrained free chains of the same size, we dissolve deuterated free chains into unlabeled PDMS networks to examine the line shapes at high extension. In the following paper,[28] we present a theoretical approach to estimate the probability distribution of segmental alignment from the entire ^{2}H NMR spectrum and apply this methodology to some of the results presented here.

Table 1. Network Compositions and Properties

M_n (g/mol)	Q	E (MPa)	w_{sol} (mass %)
5 000	3.02	1.30	0.59
11 000	3.39	1.06	0.80
36 000	4.64	0.61	1.45
90 000	7.31	0.27	5.48
30 000[a]	4.55	0.63	2.36

[a] Consists of unlabeled elastic chains and labeled probe chains, both with M_n = 30 000 g/mol. Unlabeled soluble material was extracted before dissolution of labeled free chains.

2. Experimental Procedures

2.1. Elastomer Synthesis and Characterization. PDMS chains were synthesized via anionic ring-opening of hexamethylcyclotrisiloxane.[29−31] Deuterated hexamethylcyclotrisiloxane monomer was produced using a reaction sequence adapted from Beltzung et al.[32] To conserve valuable deuterated material, these monomer crystals were mixed with hydrogenated hexamethylcyclotrisiloxane (Gelest, Inc.) before polymerization to yield randomly deuterated polymer chains.

PDMS chains were characterized using gel permeation chromatography (GPC) with polystyrene-calibrated columns. Equivalent PDMS molar masses were obtained by implementing an established conversion.[33] Partially deuterated chains with number-average molar mass of 5000, 11 000, 36 000, and 90 000 g/mol and low polydispersity (≤1.32) were end-capped with vinyl termination. These chains were cured into elastic networks by performing a hydrosilylation reaction with tetrakis(dimethylsiloxy)silane cross-linker and *cis*-dichlorobis(diethylsulfide)platinum(II) catalyst. We define the parameter r as the ratio of cross-linker arms to polymer chain ends. In accordance with past work,[34] r = 1.7 was used to create the highest quality networks for precursors of 11 000 g/mol and above. The optimum ratio is smaller for shorter precursor chains,[35] so r was reduced to 1.5 for the 5000 g/mol sample. The networks were cured in Teflon molds at 35 °C for 3 days. One unlabeled network with number-average molar mass of 30 000 g/mol (PDI = 1.27) was synthesized via the same methods with monomer purchased from Gelest.

The networks were characterized by standard swelling and extraction techniques using toluene.[36] Equilibrium mass swell ratios Q were calculated using the dry and swollen network masses. Soluble fractions w_{sol} were determined by comparison of the sample masses before and after toluene extraction. The network characteristics are summarized in Table 1. Soluble fractions were extracted from all the networks before the NMR experiments were performed. Therefore, the tested samples contained no free chains, except for the unlabeled network with dissolved probe chains. The deuterated polymer chains used as nonelastic probe chains were trimethylsiloxy end-capped and unreactive. A small amount of these chains, with M_n = 30 000 g/mol and PDI = 1.41, was spread onto the surface of the 30 000 g/mol unlabeled network. To dissolve the probe chains into the network, the sample was covered with a glass vial and placed into an oven at 65 °C for 1 week, by which time the network surfaces were completely dry. The concentration of free chains dissolved in the network was 9 wt %. After the NMR experiments were performed, a second toluene extraction was carried out to remove the deuterated probes. The network did not display a ^{2}H NMR signal after this extraction.

Samples for ^{2}H NMR measurements were cut with a razor blade into rectangular strips of approximate dimensions $32 \times 2 \times 1$ mm. Dynamic mechanical testing on these relatively small samples yielded inconsistent values for the low-strain elastic modulus E. Therefore, an empirical correlation between Q and E using unlabeled PDMS networks[34] was used to obtain E values for the deuterated networks presented in this paper.

2.2. ^{2}H NMR Methods. ^{2}H NMR data were measured on a Tecmag Apollo HF spectrometer operating at 30.72 MHz for deuterium. The NMR spectra were obtained by Fourier transforming the quadrature-detected free-induction decay after a 90° pulse of 5 μs. Each sample was centered in an 8.5 mm long rf coil at room temperature. The number of scans was increased (up to 100 000 in some cases) with increasing extension of the sample to achieve reasonable signal-to-noise ratio. The repetition delay between each scan was 1 s. A gentle line-broadening of 10 Hz was applied to the time-domain data before Fourier transformation to improve the apparent signal-to-noise ratio. Since the ^{1}H$-^2$H dipolar coupling is very weak compared to the ^{2}H quadrupolar coupling, proton decoupling was not necessary and therefore was not applied. All test pieces had uniform width and thickness to ensure uniform stretching. Stretched samples were oriented perpendicular to the 4.7 T external magnetic field and deformed using a device described in ref 37. Approximately 8 mm of material on each end of the sample was clamped into the stretching device, leaving a gauge length of about 16 mm. This was sufficient to ensure that the inner uniformly stretched portion of the sample was surrounded by the rf coil; the clamped ends were outside of the rf coil. To monitor the local extension ratio, each sample was marked with ink dots in the unstretched state. High-resolution photographs of the marked samples were taken at the rest state and for each elongation ratio once the length had stabilized. The distance between the dots was measured from each photograph, and the elongation ratio calculated by dividing the stretched distance by the unstretched distance.

3. Results and Discussion

3.1. Data Analysis: Empirical Fitting Procedure for ^{2}H NMR Spectra. As discussed in the Introduction, the incomplete averaging of the quadrupolar interaction in ^{2}H-labeled elastomers leads to non-Lorentzian line shapes. Even the spectral line shapes of samples in the unstretched state cannot be fitted to a single curve. They can, on the other hand, be well represented by a sum of two curves, each centered at zero frequency. A representative example is shown in Figure 2. The Solver tool in Microsoft Excel was implemented to fit the spectra, iterating on the height and width of each peak. Depending on the sample, the line shape was best fit by either a pair of Lorentzian curves or one Lorentzian and one Gaussian curve. For each network studied, we found that a narrow and a wide curve were required to obtain a good fit. The widths at half-height for each of these curves are denoted as γ_n and γ_w, while the signal fraction of each (integrated areas) are termed area$_n$ and area$_w$. Even though the procedure is empirical, we found that the fitting parameters for the narrow and wide curves yielded interesting information concerning the effect of the precursor molar mass on the line shape. When the samples were deformed and the spectra broadened, the fitting procedure was adjusted. Here, each spectrum was modeled by the sum of two pairs of curves, and the program also iterated on the peak distance from $\nu = 0$ for each pair of curves. Each coupled pair was constrained to have the same peak height, width, and distance from zero frequency. It is important to note that the fact that the spectra are nicely fitted to pairs of curves does not imply that each curve in a pair represents separate populations of orientations. As shown in Figures 2 and 4, the wider curve represents a population with more highly oriented segments on average (i.e., less isotropically averaged orientation on the NMR time scale) than the narrow curve, but the two curves show significant overlap of segment orientations.

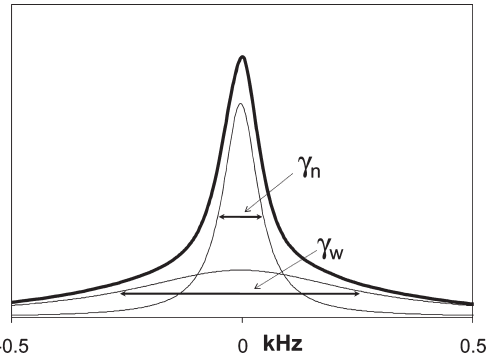

Figure 2. Empirical decomposition of the spectral line shape of an undeformed PDMS network (bold line). The experimental spectrum is well represented by the sum of a narrow curve and a wide curve (thin lines) with widths at half-height γ_n and γ_w.

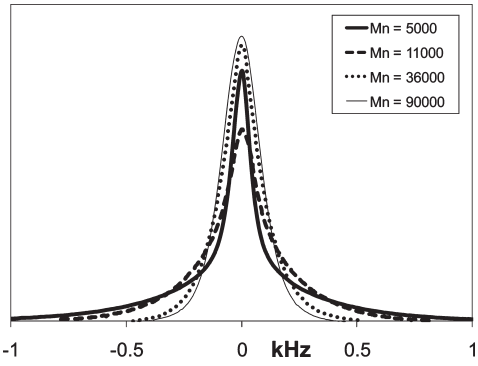

Figure 3. ^{2}H NMR spectra for undeformed 5000 (thick line), 11 000 (dashed line), 36 000 (dots), and 90 000 g/mol (thin line) networks. The line shapes are normalized by the area under each spectrum.

3.2. Evolving Line Shape in Unstretched Networks. ^{2}H NMR spectra for unstretched end-linked networks with varying precursor M_n are presented in Figure 3. The peak heights are normalized such that the area under each spectrum is identical. Each spectrum was fit to the sum of two curves using the procedures outlined in section 3.1. These fitting parameters are displayed in Table 2. Note that the signal fractions area$_n$ and area$_w$ for the unstretched networks are discussed in section 3.3. The widths at half-height for the chains in the *melt state* before cross-linking are reported as γ_{melt}. The spectra for these melts showed rather sharp Lorentzian peaks, as expected. Note the increase in γ_{melt} with increasing M_n. This reflects the higher viscosity of the longer chains, where random segment motion is slightly slower and the spectra are thus a bit broader. The observed line shape shows clear changes with the precursor molar mass M_n. The 5000 g/mol network is best represented by the typical super-Lorentzian curve (the sum of a narrow and a wide Lorentzian curve) previously reported for PDMS networks.[4] However, the form of the spectra, particularly in the wings, differs with increasing M_n. The spectra in Figure 3 demonstrate that the spectral wings are most important for networks synthesized from low molar mass precursors. For networks synthesized from precursors with $M_n = 11\,000$ g/mol and above, we found that the spectra were better modeled by a Lorentzian with

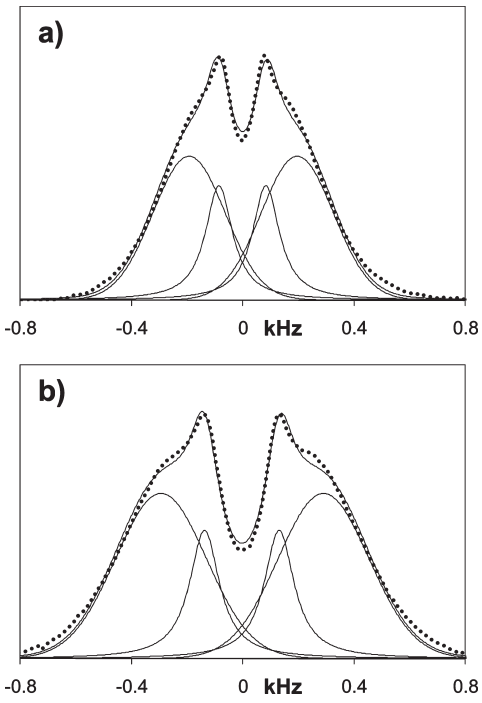

Figure 4. ^{2}H NMR spectra for 36 000 g/mol end-linked networks at (a) $\alpha = 1.98$ and (b) $\alpha = 2.56$. The experimental spectra (dots), doublet fits to each spectrum (lines), and the sum of the doublet pairs (line) are depicted. Note the appearance of a shoulder in the line shape.

Table 2. Parameters of the Fitted Curves to the Spectra of Melts and Unstretched Networks and the Estimated Fraction of Elastic Chains f_{el} in Each Network

	line width (kHz)			signal fraction		
M_n (g/mol)	γ_{melt}	γ_n	γ_w	area$_n$	area$_w$	f_{el}
5 000	0.054	0.047	0.289	0.45	0.55	0.86
11 000	0.061	0.077	0.245	0.50	0.50	0.84
36 000	0.069	0.065	0.121	0.49	0.51	0.79

narrow line width and a Gaussian with larger line width. This is a consequence of the decreasing importance of the wings of the spectra, since Gaussian functions have a sharper cutoff than the wide wings of a Lorentzian. This is also captured by the value of γ_w, which decreases steadily with increasing M_n.

To interpret these results, it is instructive to think of the spectra as the sum of time-averaged pairs of lines, as outlined in the Introduction. Therefore, each spectrum is the sum of the chain segment order parameter distribution and its image reflected across $\nu = 0$. The outer portion of the distribution, which is represented by the wings in the full spectrum of the 5000 g/mol elastomer, corresponds to segments with a higher degree of order. Computer simulations have demonstrated that the outer portions of these spectra result from chains with especially high end-to-end distances.[27] Thus, it appears that some amount of chains cross-link when in an extended state. These chains are more motionally constrained than those that attach to a constraint while still in a more coiled state. Since the wings decrease progressively with increasing precursor M_n, the distribution of segment orientations is narrower for higher molar mass elastic chains. Longer chains, then, are less perturbed from their initial, random conformations when changing from the melt state to the elastic state. This interpretation is consistent with recently reported

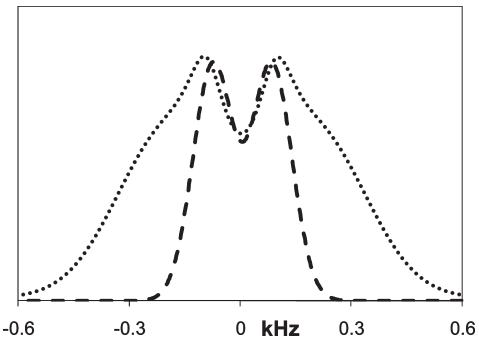

Figure 5. Comparison of the ^{2}H NMR spectra of a 36 000 g/mol labeled network at $\alpha = 2.03$ (dots) and 30 000 g/mol labeled free chains dissolved in a 30 000 g/mol unlabeled network at $\alpha = 2.05$ (dashed line). The PDMS networks have similar values of the elastic modulus E. The peak separation for the probe chains is similar to the inner doublet displayed by the network spectrum.

MQ NMR experiments[38−40] that demonstrated wider order parameter distributions for shorter elastic chain networks.

The networks synthesized from precursors with M_n up to 36 000 g/mol were high quality and had low soluble fractions upon extraction, but the soluble fraction for the 90 000 g/mol network was 5.5% (Table 1). This indicates a relatively large fraction of isotropically mobile pendant chains in this network. We use the Macosko−Miller model for nonlinear polymerization[41−43] to estimate the fraction of elastic chains f_{el} in each network (Table 2). These estimates were previously shown to agree reasonably with values of f_{el} obtained from transverse ^{2}H NMR dephasing curves that exhibit two distinguishable decay times associated with the decay times of segments of elastic chains and those of pendant chains.[44] Comparison of the signal fractions and f_{el} values (Table 2) reveals that, with the exception of the 90 000 g/mol network, the elastic chains must contribute to both the narrow curve and the wide curve. Inelastic chains contribute only to the narrow curve as is demonstrated later in Figure 5. In the case of the 90 000 g/mol network, the major contribution to the narrower curve is likely coming from the high fraction of nonelastic material in this network. Note that the constraints in this poor quality network do not restrict isotropic segment motion much, since γ_w is less than 20% larger than the melt value. Contrast this with the higher quality 36 000 g/mol network where γ_w is nearly twice γ_{melt}, indicating a significant restriction due to the cross-links. As the elastic chains shorten, the ratio γ_w/γ_{melt} increases to 4 and 5 for the 11 000 and 5000 g/mol networks, respectively.

Using the natural ^{2}H abundance in a 47 000 g/mol end-linked network, Saalwächter and Sommer observed that the spectrum was not Lorentzian and did not show long spectral wings.[40] The authors used this example to assert that the super-Lorentzian line shape is not universal for PDMS elastomers. They attributed the sharp center of this frequently observed shape to high numbers of mobile defects (soluble fraction, dangling chains, loops) in previous studies. The line shape reported for this 47 000 g/mol specimen appears qualitatively similar to the 36 000 and 90 000 g/mol spectra presented in Figure 3. Therefore, comparison with our lower M_n samples leads us to suggest that the transition from super-Lorentzian to this unexpected spectral form must be a result of the length of the elastic chains and not just the presence of inelastic defects.

3.3. Stretched Networks: Two Doublets Emerge at High Extension. End-linked networks synthesized from low-M_n precursor chains are brittle and thus difficult to stretch to

high extension before fracture. Our 36 000 and 90 000 g/mol networks proved compliant, however, and could be stretched to more than twice their initial lengths. A doublet in the NMR spectrum emerges with uniaxial extension, as depicted in Figure 1. We observed this expected pattern upon slight extension of our 5000 and 11 000 g/mol samples. The 36 000 g/mol network, meanwhile, began to show a more complex line shape at high extension. Spectra for this network at $\alpha = 1.98$ and 2.56 are displayed in Figure 4. At these high states of strain, a shoulder appears on the outer edge of each doublet. To our knowledge, such a ^{2}H NMR spectral form has not been previously observed in stretched PDMS networks.

To analyze this spectral shape, we fit the line shape to two pairs of peaks. We term the peak splitting for the wide and narrow doublet $\Delta\nu_w$ and $\Delta\nu_n$, respectively. As in section 3.2, the signal fractions of the wide and narrow curves are denoted area$_w$ and area$_n$. The outer shoulders are better fit to Gaussian curves, while the inner splitting is modeled by a pair of narrow Lorentzians. The observed shape is consistent with the spectral shape of the unstretched network depicted in Figure 3 (a single wider Gaussian and a single narrower Lorentzian). This suggests that the initial undeformed conformation of the cross-linked chains has some effect on the segment alignment at high strain.

To attempt to identify the contributions to the outer and inner peaks, we examined the spectra of dissolved free chain samples with increasing extension. Any anisotropic ordering of the segments of these chains can only result from interchain couplings between elastic chains and free chains. A comparison of the spectra of a labeled network and labeled free chains at similar elongation is shown in Figure 5. Both the labeled network and the host network for the free chains have similar values of the elastic modulus (Table 1). From Figure 5, it is clear that the probe chain spectrum shows a single doublet when highly strained. This pair of peaks with separation $\Delta\nu_p$ roughly corresponds to the inner doublet pair $\Delta\nu_n$ displayed by the ^{2}H-labeled network. The outer shoulders from the network spectrum are absent for the free chains. Thus, the wider pair of peaks with splitting $\Delta\nu_w$ must result from the cross-link constraints placed on the elastic chains. The outer tails of these spectra correspond to segments that are on-average quite aligned along the end-to-end distance. If we assign the wider curve to segments of chains that were cross-linked in a state of high end-to-end distance, then this population of chains has also segments that are not highly oriented because the wider curve covers a large range of small frequency shifts. A comparison of both $\Delta\nu_n$ and $\Delta\nu_w$ for the cross-linked network with the single peak splitting $\Delta\nu_p$ displayed by the probe chains vs $\alpha^2 - 1/\alpha$ is presented in Figure 6. Note the close correspondence of the probe chain splitting with the narrower splitting of the elastomer.

Average signal fractions of the stretched networks are presented in Table 3. These integrated areas are constant with increasing stretch ratio and in general show a good match with area$_w$ and area$_n$ for the unstretched networks (Table 2). The area$_w$ value is noticeably larger for the stretched networks in the 36 000 g/mol network, but this is likely due to the difficulty of fitting the unstretched network to two overlapping curves. Since the respective contributions to the narrow and wide curves are essentially equal across all elongation ratios, the number of chain segments in each population does not change as the networks are stretched. This is consistent with our interpretation that the outer population is the result of chains trapped during the curing in an extended conformation. While the degree

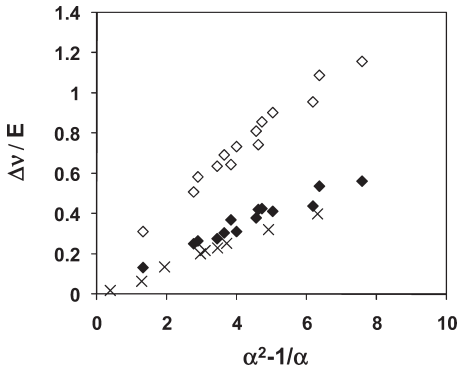

Figure 6. Peak separations normalized by elastic modulus vs $\alpha^2 - 1/\alpha$. Diamonds represent splitting of the outer doublet ($\Delta\nu_w$, open symbols) and inner doublet ($\Delta\nu_n$, filled symbols) for the 36 000 g/mol labeled network. × corresponds to labeled free chains dissolved in an unlabeled 30 000 g/mol network ($\Delta\nu_p$). Note the close match of the $\Delta\nu_n$ and $\Delta\nu_p$ data.

Table 3. Average Signal Fractions of the Narrow and Wide Curves in Stretched Networks

	signal fraction		
M_n (g/mol)	area$_n$	area$_w$	stdev
5 000	0.46	0.54	0.02
11 000	0.51	0.49	0.04
36 000	0.35	0.65	0.05
90 000	0.26	0.74	0.14

of segmental ordering changes with elongation ratio, the number of segments belonging to each chain population should not.

The previously unreported line shape observed here supports the models detailed in the Introduction. Specifically, these models have divided the line shape into contributions from network constraints and chain interaction.[16−19] As demonstrated in previous experiments[11] and analytical studies[45] and shown in Figure 6, there is a correlation between the classically reported $\Delta\nu_n$ values of network chains and unattached free chains. This anisotropic ordering, which is easily monitored by the splitting displayed in ^{2}H NMR spectra upon strain, results from excluded volume interactions. Our results show that the contribution to the ^{2}H NMR signal from the network constraints can become observable separately from the purely excluded volume effect at high extension. The models[16−19] predict that the line shape for noninteracting phantom networks will simply broaden without splitting upon increasing strain. Therefore, the wider spectral splitting $\Delta\nu_w$ should not imply a splitting independent of the effect of excluded volume interactions. The more highly stretched network chains that contribute to the outer shoulder in the spectra must (rather obviously) interact with other chain segments while preferentially orienting along the strain axis. Thus, it appears that this population of ordered segments is subject to an additional inherent potential imposed by the cross-linking that leads to chains with more extended end-to-end distances. The inner splitting can then be interpreted as a result of segmental ordering due to excluded volume interactions of both elastic chains *and* defects such as pendant chains and loops.

To connect to the theoretical models, we can compare the slopes of the $\Delta\nu_n$ and $\Delta\nu_w$ data shown in Figure 6. For the outer doublet $(\Delta\nu/E)/(\alpha^2 - 1/\alpha) = 0.104$ kHz/MPa vs 0.050 for the narrow doublet. This yields a $\Delta\nu_w/\Delta\nu_n$ ratio of 2.08.

In ref 19, the average segment alignment due to the constraints and mean field (i.e., the excluded volume interaction)

are termed $P_2(\cos\theta)_R$ and $P_2(\cos\theta)_V$, respectively. According to this model, these can be calculated by

$$P_2(\cos\theta)_R = \frac{1}{3N}\left(\alpha^2 - \frac{1}{\alpha}\right) \quad (4)$$

$$P_2(\cos\theta)_V = \frac{1}{15N\pi}\frac{b}{\xi}\left(\alpha^2 - \frac{1}{\alpha}\right) \quad (5)$$

where N is the number of statistical segments of size b between each junction and ξ is the Edwards screening length. For PDMS, the ratio b/ξ has been estimated to be 4.[45] Thus, the model predicts $P_2(\cos\theta)_R/P_2(\cos\theta)_V = 3.9$, almost twice our calculated $\Delta\nu_w/\Delta\nu_n$ ratio. We suspect that the primary reason for the discrepancy is the model's assumption of affine deformation at the molecular scale. Since the actual chain deformation is subaffine, we expect less segmental alignment than predicted by the above model. Another factor that may contribute to this discrepancy is the empirical fitting procedure used on the experimental spectra. While $\Delta\nu_w$ and $\Delta\nu_n$ were calculated from the peak locations of the curves used to fit the data, the average degree of order of a distribution does not always correspond with the peak position. We expect that the outer tails of these spectra might lead to higher average values of segmental order than measured by the peak locations.

4. Conclusions

^{2}H NMR line shapes of end-linked networks evolve with precursor chain molar mass. We analyzed these spectra for unstretched and stretched elastomers to elucidate information about ordering of chain segments. Short-chain end-linked networks exhibit wide spectral wings in the ^{2}H NMR line shape caused by segments from chains that were cross-linked in a state of large end-to-end distance. These wings form the super-Lorentzian line shape commonly reported for PDMS elastomers in the unstrained state. This residual segmental orientation is quantified by the larger peak width at half-height of the short chain networks as compared to the un-cross-linked precursors. The distribution of order parameters in networks with longer precursor chains is more uniform. The line shape of the labeled networks made from larger molar mass precursors is pseudo-Gaussian, exhibiting a broader center and a less prominent contribution from the high-frequency wings. Fewer of these longer chains are cross-linked in an extended state, and their perturbation from their random melt conformations is less significant than for end-linked shorter precursors.

When long-chain elastomer samples are highly stretched, the line shape can exhibit clear shoulders in addition to the commonly observed narrow doublet peaks. A good fit to the spectrum is obtained using two distributions of frequency shifts representing different populations of segment orientations. Both populations become more ordered with increasing strain, but we find that the contribution of each population to the spectrum remains, with one exception, practically constant. Since the narrower spectral split can be mimicked by labeled free chains dissolved in an unlabeled network, it represents the effect of excluded volume interactions between segments as has been previously established. We show that this central narrower contribution to the spectrum comes from both elastic chains and nonelastic defects by demonstrating that for model networks with relatively few defects it represents about 50% of the spectrum. We also deduced that the more highly ordered chain segments are the result of elastic constraints induced during the cross-linking.

Networks with lower mass precursors could not be deformed to high extension. In the limited elongation ratios we were able to access for the 5000 and 11 000 g/mol networks, it was not possible to observe a clear outer doublet. It appears that the chain segment orientations that are highly influenced by the cross-linking contribute to the long spectral wings here, which widen further upon deformation but cannot be separated into a second doublet at the elongation ratios accessible before fracture.

These changes in line shape with molar mass in both the stretched and unstrained state demonstrate the wealth of information contained in the entire spectrum. While the fitting procedure detailed here to analyze the ^{2}H NMR spectrum of an elastomer provides qualitative insights into the distributions of segment orientations, it is often desirable to measure the average segmental alignment of a sample and generate the full probability distribution of orientation. In the following paper we develop an approach based on the maximum entropy method that allows for estimation of these properties directly from each spectrum.[28]

Acknowledgment. This work was supported by the National Science Foundation Polymers Program under Grant DMR-0705565. We thank Bernardo Aguilera-Mercado and Fernando Escobedo for numerous helpful discussions.

References and Notes

(1) Abragam, A. *The Principles of Nuclear Magnetism*; Clarendon Press: Oxford, 1961.
(2) Deloche, B.; Samulski, E. T. *Macromolecules* **1981**, *14*, 575–581.
(3) Deloche, B.; Beltzung, M.; Herz, J. *J. Phys., Lett.* **1982**, *43*, 763–769.
(4) Gronski, W.; Stadler, R.; Jacobi, M. M. *Macromolecules* **1984**, *17*, 741–748.
(5) Dubault, A.; Deloche, B.; Herz, J. *Polymer* **1984**, *25*, 1405–1410.
(6) Gronski, W.; Emeis, D.; Brüderlin, A.; Jacobi, M. M.; Stadler, R. *Br. Polym. J.* **1985**, *17*, 103–110.
(7) Toriumi, H.; Deloche, B.; Herz, J.; Samulski, E. T. *Macromolecules* **1985**, *18*, 304–305.
(8) Deloche, B.; Dubault, A.; Herz, J.; Lapp, A. *Europhys. Lett.* **1986**, *1*, 629–635.
(9) Sotta, P.; Deloche, B.; Herz, J.; Lapp, A.; Durand, D.; Rabadeux, J. C. *Macromolecules* **1987**, *20*, 2769–2774.
(10) Kornfield, J. A.; Chung, G.; Smith, S. *Macromolecules* **1992**, *25*, 4442–4444.
(11) McLoughlin, K.; Waldbieser, J. K.; Cohen, C.; Duncan, T. M. *Macromolecules* **1997**, *30*, 1044–1052.
(12) Mark, J. E.; Erman, B. *Rubberlike Elasticity: A Molecular Primer*; Wiley-Interscience: New York, 1988.
(13) Jelinski, L. *Annu. Rev. Mater. Sci.* **1985**, *15*, 359–377.
(14) Flory, P. J. *Principles of Polymer Chemistry*; Cornell University Press: Ithaca, NY, 1953.
(15) Kuhn, W.; Grün, F. *Kolloid Z.* **1942**, *101*, 248–271.
(16) Sotta, P.; Deloche, B. *Macromolecules* **1990**, *23*, 1999–2007.
(17) Brereton, M. G. *Macromolecules* **1993**, *26*, 1152–1157.
(18) Warner, M.; Callaghan, P. T.; Samulski, E. T. *Macromolecules* **1997**, *30*, 4733–4736.
(19) Ries, M. E.; Brereton, M. G.; Klein, P. G.; Ward, I. M.; Ekanayake, P.; Menge, H.; Schneider, H. *Macromolecules* **1999**, *32*, 4961–4968.
(20) Depner, M.; Deloche, B.; Sotta, P. *Macromolecules* **1994**, *27*, 5192–5199.
(21) Sotta, P.; Higgs, P. G.; Depner, M.; Deloche, B. *Macromolecules* **1995**, *28*, 7208–7214.
(22) Sotta, P. *Macromolecules* **1998**, *31*, 8417–8422.
(23) Poon, C.; Samulski, E. T. *Makromol. Chem., Macromol. Symp.* **1990**, *40*, 109–120.
(24) Poon, C.; Samulski, E. T. *J. Non-Cryst. Solids* **1991**, *131*, 509–515.
(25) Gronski, W.; Forster, F.; Pyckhout-Hintzen, W.; Springer, T. *Makromol. Chem., Macromol. Symp.* **1990**, *40*, 121–137.
(26) Sotta, P. *Macromolecules* **1998**, *31*, 3872–3879.
(27) Yong, C. W.; Higgs, P. G. *Macromolecules* **1999**, *32*, 5062–5071.
(28) Aguilera-Mercado, B. M.; Cohen, C.; Escobedo, F. *Macromolecules* **2009**, DOI: 10.1021/ma9017179.
(29) Lee, C. L.; Johannson, O. K. *J. Polym. Sci., Polym. Chem.* **1976**, *14*, 729–742.

(30) Lee, C. L.; Marko, O. W.; Johannson, O. K. *J. Polym. Sci., Polym. Chem.* **1976**, *14*, 743–758.
(31) Genesky, G. D.; Aguilera-Mercado, B. M.; Bhawe, D. M.; Escobedo, F. A.; Cohen, C. *Macromolecules* **2008**, *41*, 8231–8241.
(32) Beltzung, M.; Picot, C.; Rempp, P.; Herz, J. *Macromolecules* **1982**, *15*, 1594–1600.
(33) Lapp, A.; Herz, J.; Strazielle, C. *Makromol. Chem.* **1985**, *186*, 1919–1934.
(34) Patel, S. K.; Malone, S.; Cohen, C.; Gillmor, J.; Colby, R. *Macromolecules* **1992**, *25*, 5241–5251.
(35) Takahashi, H.; Shibyama, M.; Fujisawa, H.; Noruma, S. *Macromolecules* **1995**, *28*, 8824–8828.
(36) Weiss, P.; Herz, J.; Rempp, P. *Makromol. Chem.* **1970**, *135*, 249–261.
(37) Hedden, R. C.; Tachibana, H.; Duncan, T. M.; Cohen, C. *Macromolecules* **2001**, *34*, 5540–5546.
(38) Saalwächter, K.; Ziegler, P.; Spyckerelle, O.; Haidar, B.; Vidal, A.; Sommer, J.-U. *J. Chem. Phys.* **2003**, *119*, 3468–3482.
(39) Saalwächter, K.; Kleinschmidt, F.; Sommer, J.-U. *Macromolecules* **2004**, *37*, 8556–8568.
(40) Saalwächter, K.; Sommer, J.-U. *Macromol. Rapid Commun.* **2007**, *28*, 1455–1465.
(41) Macosko, C. W.; Miller, D. R. *Macromolecules* **1976**, *9*, 199–206.
(42) Miller, D. R.; Macosko, C. W. *Macromolecules* **1976**, *9*, 206–211.
(43) Miller, D. R.; Valles, E. M.; Macosko, C. W. *Polym. Eng. Sci.* **1979**, *19*, 272–283.
(44) McLoughlin, K.; Szeto, C.; Duncan, T. M.; Cohen, C. *Macromolecules* **1996**, *29*, 5475.
(45) Brereton, M. G.; Ries, M. E. *Macromolecules* **1996**, *29*, 2644–2651.